Check for updates

Photopolymerisation | Very Important Paper

International Edition: DOI: 10.1002/anie.201912608
German Edition: DOI: 10.1002/ange.201912608

# A Versatile 3D and 4D Printing System through Photocontrolled RAFT Polymerization

*Zhiheng Zhang*[+], *Nathaniel Corrigan*[+],* *Ali Bagheri, Jianyong Jin, and Cyrille Boyer**

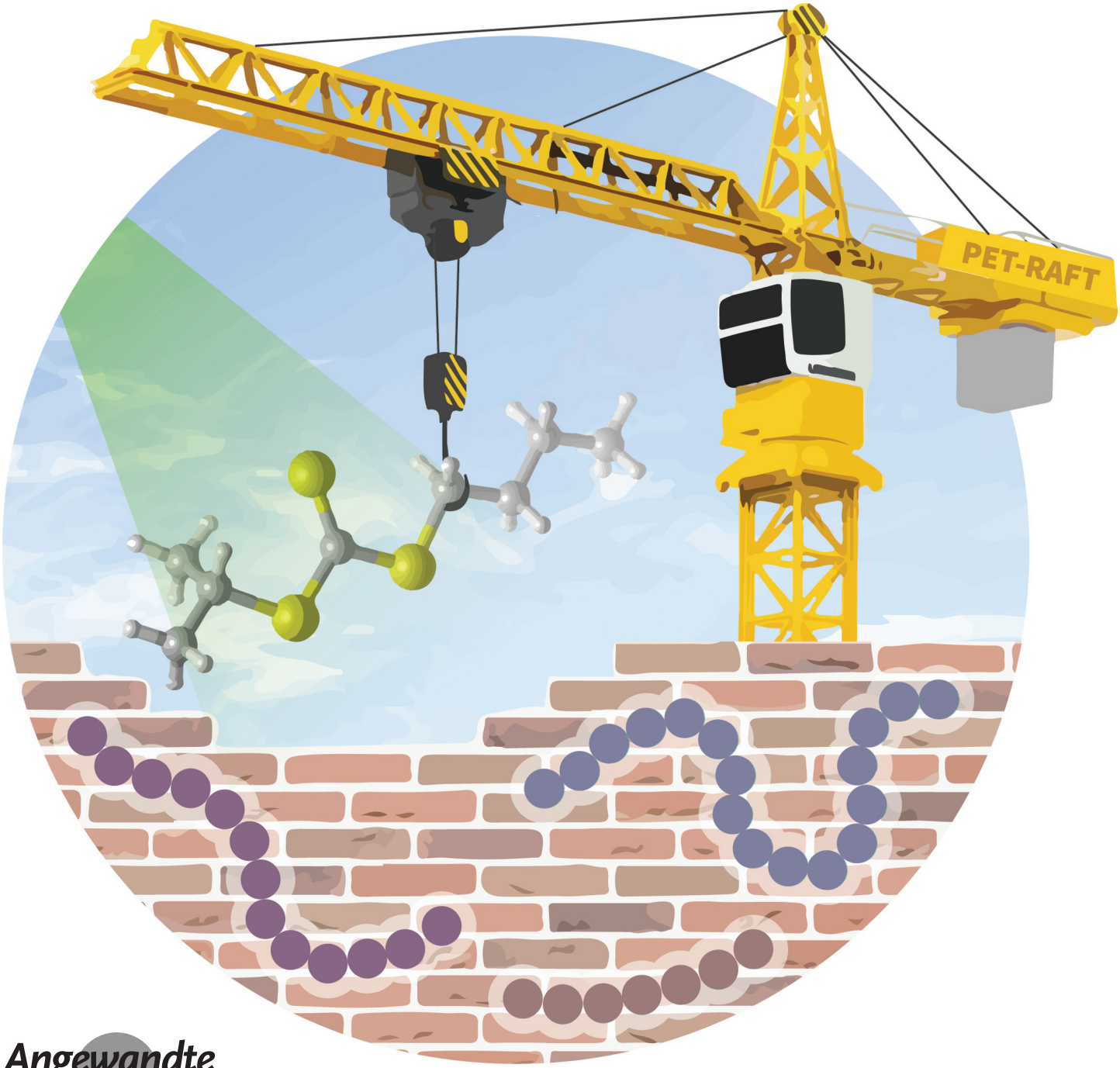



© 2019 Wiley-VCH Verlag GmbH & Co. KGaA, Weinheim

***Abstract:*** *Reversible addition-fragmentation chain-transfer (RAFT) polymerization is a valuable tool for synthesizing macromolecules with controlled topologies and diverse chemical functionalities. However, the application of RAFT polymerization to additive-manufacturing processes has been prevented due to the slow polymerization rates of typical systems. In this work, we developed and optimized a rapid visible (green) light mediated RAFT polymerization process and applied it to an open-air 3D printing system. The reaction components are non-toxic, metal free and environmentally friendly, which tailors these systems toward biomaterial fabrication. The inclusion of RAFT agent in the photosensitive resin provided control over the mechanical properties of 3D printed materials and allowed these materials to be post-functionalized after 3D printing. Additionally, photoinduced spatiotemporal control of the network structure provided a one-pass approach to 4D printed materials. This RAFT-mediated 3D and 4D printing process should provide access to a range of new functional and stimuli-responsive materials.*

## Introduction

The development of additive manufacturing techniques over the past 30 years has had an immeasurable impact on materials science.[1] Compared to traditional subtractive manufacturing, additive manufacturing has allowed the production of materials with arbitrary geometries while minimizing waste, and has provided non-experts access to complex materials. Among the most common 3D printing techniques (fused filament fabrication (FFF), 3D inkjet printing, etc.) photoinduced processes have garnered significant attention, largely due to the inherent benefits of light as an external stimuli, including temperature insensitivity, high biocompatibility, and spatiotemporal control; 3D printing via stereolithography (SLA), projection microstereolithography (PμSL), and digital light processing (DLP) techniques all exploit the ability for light to be constrained in a well-defined region to produce geometrically complex objects.[2] Moreover, the extensive range of photochemistry available to perform photoinduced polymerization has provided materials with diverse physical and chemical properties.

Recently, some interesting 3D and 4D printing techniques have been developed by several research groups that exploit the unique attributes of light to produce complex materials.[3] For instance, Hawker and co-workers developed a new approach for visible light controlled 3D printing based on the bleaching of photochromic molecules, which allowed large cure depths and printed materials devoid of layer defects.[3c] Notably, the use of a single resin formulation containing both cationic and radically sensitive components enabled one step printing of multimaterial objects. Schwartz and Boydston have also demonstrated a dual wavelength 3D and 4D printing approach that activated dual cationic and radical polymerizations under UV and visible irradiation wavelengths, respectively.[3d] The use of a multi-wavelength DLP system provided 4D printed materials with tailored anisotropic properties that showed swelling induced actuation based on the spatial confinement of each wavelength during the one-pass layer-by-layer printing process. In other works by Dunn, Ge and co-workers, the independence of thermal and photo-induced chemistry was utilized for 3D printed multimaterial, shape memory, and reprocessable polymers.[3f,4] In these examples, the use of light to 3D print the initial objects enabled the secondary material transformations to be independently activated.

Concurrently with the expansion of 3D and 4D printing techniques, the development of reversible deactivation radical polymerization (RDRP) and other controlled polymerization techniques over the past 20 years has provided polymer chemists with new tools to enact macromolecular syntheses.[5] Particularly, reversible addition-fragmentation chain transfer (RAFT) polymerization techniques have been extensively studied due to their ability to produce well-defined macromolecules with diverse architectures and chemical functionalities under a wide range of conditions.[6] RAFT polymerization utilizes a degenerative chain transfer process between propagating radicals and thiocarbonylthio species (RAFT agents),[5b,6c,7] which allows a large fraction of the growing polymer chains to remain dormant. The key for synthesizing architecturally diverse polymers via these approaches lies in the retention of the thiocarbonylthio polymer chain-end throughout the polymerization; repeated activation of the dormant thiocarbonylthio-capped polymer chain via transfer reactions, and subsequent monomer additions allow the formation of all manner of block, graft, and branched copolymers.

More recently, photocontrolled RAFT polymerization processes have been developed that display the favorable properties of RAFT polymerization while being activated with benign, low energy visible light.[8] Notably, our group developed a photocatalyzed polymerization process termed photoinduced electron/energy transfer-RAFT (PET-RAFT) polymerization.[9] In PET-RAFT polymerization, a photocatalyst is excited under visible or near-infrared light irradiation, and subsequently transfers an electron or energy to a thiocarboylthio species. The thiocarbonylthio species can then fragment to produce a radical capable of initiating radical polymerization.[10] PET-RAFT polymerization exhibits outstanding tolerance to molecular oxygen and can produce polymers under a broad range of conditions with high retention of the thiocarbonylthio chain-end. The high chain-end fidelity of polymeric networks synthesized through these and other photoinduced RAFT processes have also

[*] Z. Zhang,[+] Dr. N. Corrigan,[+] Prof. Dr. C. Boyer
Centre for Advanced Macromolecular Design and Australian Centre for NanoMedicine, School of Chemical Engineering, University of New South Wales
Sydney, NSW 2052 (Australia)
E-mail: n.corrigan@unsw.edu.au
cboyer@unsw.edu.au
Dr. A. Bagheri, Dr. J. Jin
School of Chemical Sciences, The University of Auckland, and Dodd-Walls Centre for Quantum and Photonic Technologies
Auckland 1010 (New Zealand)
[+] These authors contributed equally to this work.

Supporting information and the ORCID identification number(s) for the author(s) of this article can be found under https://doi.org/10.1002/anie.201912608.

 © 2019 Wiley-VCH Verlag GmbH & Co. KGaA, Weinheim 

15213773, 2019, 50, Downloaded from https://onlinelibrary.wiley.com/doi/10.1002/anie.201912608 by University Of New England, Wiley Online Library on [20/07/2023]. See the Terms and Conditions (https://onlinelibrary.wiley.com/terms-and-conditions) on Wiley Online Library for rules of use; OA articles are governed by the applicable Creative Commons License

been exploited to expand the functionality of pre-formed materials.[11] For instance, Johnson and co-workers presented an elegant strategy for modifying "parent" polymer networks containing trithiocarbonate units within the polymer backbone.[11a] Under blue light irradiation in the presence of solutions containing a photoredox catalyst and monomer, the trithiocarbonate units were able to be activated, leading to polymerization and modification of the original network. This network post-functionalization provided "daughter" gels with variable properties.

Additionally, other thiocarbonylthio functional groups capable of degenerative chain transfer have been used in polymeric materials to modify the as-formed network structures. Matyjaszewski and co-workers showed an early example of a trithiocarbonate mediated network rearrangement process.[12] Remarkably, the butyl acrylate networks were able to be cut and subsequently fused together under UV light irradiation via photoinduced degenerative transfer between the trithiocarbonate functionalities in each network fragment. Similarly, dithiocarbamates have been used by Kloxin and co-workers to relieve stress, and induce self-healing behaviour within networks via bond rearrangement processes under UV light.[13] Notably, this example utilized the spatial control possible with light to induce a secondary photopatterning of the original material. Although these methods demonstrate that RAFT agents can be incorporated into networks for rich post-modification procedures, the slow polymerization rate for typical RAFT polymerization (and other RDRP) processes has precluded their direct application to 3D printing processes. As 3D printing processes require a rapid cure time for practical applications, 3D printing of polymeric materials is generally conducted using comparatively rapid free-radical or cationic polymerizations. As such, 3D printing via RAFT polymerization has remained a great challenge and is receiving attention from various research groups, including our own. For instance, Jin, Bagheri and co-workers in collaboration with Boyer's group, very recently developed a photoiniferter based 3D printing process via direct photolysis of trithiocarbonates under 405 nm irradiation. Due to the nature of the photoiniferter mechanism, this 3D printing process was conducted in an inert atmosphere.[14a] To extend the viability of RAFT based 3D printing, a parallel collaboration between our groups has also very recently investigated 3D printing using a PET-RAFT process to activate trithiocarbonates under fully open to air conditions and achieve a relatively faster printing.[14b]

Herein, we investigate 3D and 4D printing via photoinduced RAFT polymerization (PET-RAFT 3D and 4D printing using an organic photocatalyst) activated under visible light ($\lambda_{max} = 525$ nm, intensity $= 0.32$ mW cm$^{-2}$. The photocatalytic system featured an organic dye (Erythrosin B, EB) and a tertiary amine co-catalyst (triethanolamine), which allowed 3D printing to be conducted in aqueous solutions without prior deoxygenation. Following fabrication and mechanical testing of the 3D printed materials, the trithiocarbonate groups incorporated in the networks were activated under visible light for post-modification processes. The dormant RAFT-capped polymer chains were able to be reinitiated in the presence of EB under green light irradiation, which enabled surface modification of the 3D printed objects. Additionally, the use of light allowed the formation of materials with spatially tailored properties to be printed in a single step, which provided an avenue to print 4D materials through swelling and dehydration induced actuation.

## Results and Discussion

### Optimization of resin formulations

In the development of our RAFT mediated photopolymerization process, we initially prioritized increasing the polymerization rate such that application to open-air vat 3D printing systems would provide practical printing speeds. Based on our previous experience with organic dyes as photocatalysts (PCs) for PET-RAFT polymerization, we initially tested two xanthene based dyes, namely eosin Y (EY) and erythrosin B (EB), for their ability to mediate rapid polymerization under green light in the presence of air.[14–15] EY is frequently used as a biological stain, and has also previously been used to initiate free-radical polymerization in the presence of tertiary amines as co-catalysts via a type II photoinitiation mechanism, as well as other organic synthetic transformations.[16] The structurally similar EB has been used by our group for PET-RAFT polymerization, where it was determined to be a more effective PC compared to EY and similar halogenated xanthene dyes, such as phloxine B and rose bengal, due to its favorable photophysical and electrochemical properties, including a higher triplet quantum yield ($\Phi_T$), decreased fluorescence quantum yield ($\Phi_F$), and a higher excited state reduction potential ($E^0(PC^{\bullet+}/^3PC^*)$).[15b,c] In addition to the organic dye as PC, we also included a tertiary amine as co-catalyst in this system as these formulations have previously shown the ability to mediate rapid PET-RAFT polymerization.[15e] The inclusion of tertiary amines increases the polymerization rate by providing more energetically favorable photoinduced electron transfer (PET) processes under green light irradiation.[15d,17]

The reaction components and proposed mechanism of this photopolymerization process are shown in Figure 1; after excitation by visible light, the photocatalyst can be reduced by tertiary amines, generating a reduced PC and a corresponding tertiary amine radical cation (Figure 1 B). The reduced PC can then transfer an electron to the RAFT agent, returning the PC to the ground state. The reduced RAFT species subsequently undergoes β-scission of the weak C-S bond to generate a thiocarbonylthio stabilized anion species and a radical propagating species ($P_n^{\bullet}$) capable of adding across monomer vinyl bonds. The propagating radical species can interact with other thiocarbonylthio species and chain growth is regulated by the regular RAFT mechanism.[6b] Recombination of the propagating radical with the anionic thiocarbonylthio species and further electron transfer to oxygen or tertiary amine radical cations closes the catalytic cycle. Notably, molecular oxygen present in the reaction mixture can be consumed by electron transfer reactions from the reduced PC species or the anionic RAFT agent, as was proposed by Qiao and co-workers.[15a,18] Although another

 © 2019 Wiley-VCH Verlag GmbH & Co. KGaA, Weinheim 

15213773, 2019, 50, Downloaded from https://onlinelibrary.wiley.com/doi/10.1002/anie.201912608 by University Of New England, Wiley Online Library on [20/07/2023]. See the Terms and Conditions (https://onlinelibrary.wiley.com/terms-and-conditions) on Wiley Online Library for rules of use; OA articles are governed by the applicable Creative Commons License

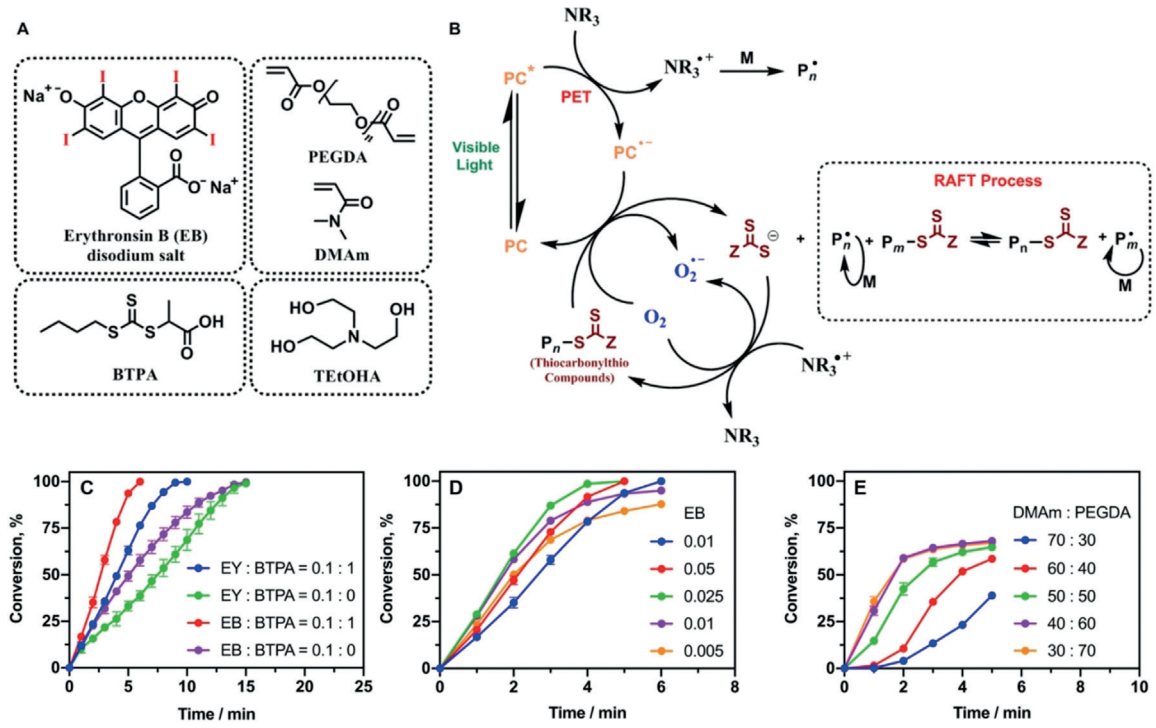


***Figure 1.*** Thiocarbonylthio containing photopolymerization resins. A) Reaction components; B) proposed PET-RAFT mechanism. PC: photocatalyst; $NR_3$: tertiary amine; PET: photoinduced electron transfer; C) comparison of vinyl bond conversions for photopolymerizations performed in the presence of EY or EB as photocatalyst, with varied molar ratios of BTPA as RAFT agent; D) vinyl bond conversion vs. time for varied EB:BTPA ratios at a fixed molar concentration of [DMAm]:[PEGDA]:[BTPA]:[TEtOHA] = 1000:50:1:20, using a solids content of 50 wt-%; (E) vinyl bond conversions vs. time for varied [DMAm]:[PEGDA] ratios at a ratio of [EB]:[BTPA]:[TEtOHA] = 0.01:1:20, performed in bulk with fixed EB, BTPA, and TEtOHA concentrations. Note: All reactions were performed under green light ($\lambda_{max}$ = 530 nm and intensity = 4.3 mW cm$^{-2}$).

mechanism involving direct electron transfer from the excited state PC to the RAFT agent is possible, the inclusion of tertiary amines in these mixtures favors the reductive PET-RAFT process shown in Figure 1 B.[15d]

For the initial model polymerizations, *N*,*N*-dimethylacrylamide (DMAm) and poly(ethylene glycol) diacrylate (PEGDA, average $M_n$ = 250 g mol$^{-1}$) were used as monomer and crosslinker, respectively. 2-(Butylthiocarbonothioylthio) propanoic acid (BTPA) was selected as RAFT agent and triethanolamine (TEtOHA) was used as a tertiary amine co-catalyst, and the reaction was performed in water at a total solids content of 50 wt-%. The initial ratio of [DMAm]:[PEGDA]:[BTPA]:[TEtOHA] was 1000:50:1:20 and the ratio of catalyst (EY or EB) to BTPA was either 0.1:1 or 0.1:0. The model polymerizations were conducted in open-air droplets (20 μL) under 4.3 mW cm$^{-2}$ green light ($\lambda_{max}$ = 530 nm) irradiation. We monitored the polymerization kinetics of these systems under different conditions by following the disappearance of peak assigned to the vinylic =C–H out of plane bending mode in ATR-FTIR spectroscopy (Supporting information, Characterization). Particularly, the vinyl bond conversions after 1 min ($\alpha_{1min}$) and 4 mins ($\alpha_{4min}$) were used as a comparative guide; we reasoned that systems that present faster rates in the early stages of the polymerization (i.e., high $\alpha_{4min}$ values), and those that present negligible induction periods ($\alpha_{1min}$), would be more suitable for implementation in 3D printing processes. This is particularly pertinent in 3D printing conducted in open-air vats, where the concentration of molecular oxygen is required to be reduced to a critical concentration prior to the onset of polymerization.[3i,k,19]

The evolution of vinyl bond conversions with time for the initial reactions, as determined by online FTIR spectroscopy, are shown in Figure 1 C. The catalytic system using EB provided faster polymerization rates compared to EY for all analogous recipes due to its favorable photocatalytic properties (Supporting information, Figure S2). Unexpectedly, however, the presence of BTPA in both systems provided a noticeable rate increase compared to systems that did not include the thiocarbonylthio species. The rate increase observed with the addition of RAFT agent can be attributed to an additional reaction pathway, that is, reduction of the RAFT agent by the radical anion PC species formed after photoreduction by the tertiary amine. Recently, Sikes and co-workers proposed a photochemical mechanism for the regeneration of ground state EY based on oxidation of the EY radical anion by molecular oxygen;[20] as the thiocarbonylthio species is also capable of oxidizing the dye radical anion species, the regeneration of the ground state PC for further catalytic cycles should also be present in our system. Interestingly, in the absence of BTPA and TEtOHA the polymerization still proceeded, albeit it at a much slower rate compared to the other systems (Supporting information, Figure S2).

Given that EB provided faster polymerization kinetics compared to EY in the model reactions, we subsequently investigated the effect of altering the other reaction compo-

 © 2019 Wiley-VCH Verlag GmbH & Co. KGaA, Weinheim 

15213773, 2019, 50, Downloaded from https://onlinelibrary.wiley.com/doi/10.1002/anie.201912608 by University Of New England, Wiley Online Library on [20/07/2023]. See the Terms and Conditions (https://onlinelibrary.wiley.com/terms-and-conditions) on Wiley Online Library for rules of use; OA articles are governed by the applicable Creative Commons License

nents on the polymerization rate. The initial experiments performed with varying concentrations of TEtOHA showed that the ratio of [EB]:[BTPA]:[TEtOHA] of 0.1:1:20 provided the fastest polymerization after 4 mins irradiation (Supporting information, Table S1). As such, the ratio of [BTPA]:[TEtOHA] = 1:20 was fixed while the catalyst concentration was varied. As shown in Figure 1D, the polymerization proceeded efficiently with EB:BTPA ratios between 0.1 and 0.005, and the fastest polymerization occurred with a ratio of 0.025:1. Additionally, there was only a modest rate difference between this system and the system containing 2.5 times less EB ([EB]:[BTPA] = 0.01:1, Supporting information, Table S2 and Figure S3). The solids content in these model reactions was also varied between 25, 50, and 75 wt-% while changing the TEtOHA ratio and EB ratio relative to RAFT agent. Polymerization proceeded in all cases with the 50 wt-% system providing the fastest rates (Supporting information, Figure S4 and Table S3).

Encouragingly, these green light mediated model photopolymerizations presented rapid cure times under low energy ($I_0 = 4.3\ mW\,cm^{-2}$) green light. Prior to implementation in the 3D printing setup, we altered the ratio of monomer to crosslinker to tailor toward high modulus, free-standing materials once printed. Figure 1E shows the polymerization rate under various ratios of DMAm:PEGDA, using constant concentrations and ratios of [EB]:[BTPA]:[TEtOHA] = 0.01:1:20 (Supporting information, Methods). These reactions were performed in bulk to more closely match the prospective 3D printing conditions. Interestingly, the monomer conversions in these polymerizations did not surpass 70%; this may be due to the formation of a rigid network in the early stages of polymerization, and the inability of the pendent double bonds from PEGDA to participate in further reaction on the time scales investigated.[21] Regardless, we noticed that the polymers produced with higher concentrations of PEGDA were free standing after the droplet polymerization, which is to be expected given the higher network connectivity compared to the systems with higher molar fractions of DMAm. The polymerization performed in bulk presented relatively slow rates when the [DMAm]: [PEGDA] ratio was above 70:30 and there was solubility issues below a ratio of 30:70 (Supporting information, Table S4). Comparatively, polymerization using a 50 wt-% formulation presented fast polymerization rates with the vinyl bond conversion surpassing 88% after 4 minutes for ratios of DMAm: PEGDA between 95:5 and 70:30 (Supporting information, Figure S5). Higher concentrations of PEGDA resulted in solubility issues in the 50 wt-% system.

### *Controlling mechanical properties of RAFT-containing 3D-printed materials*

Having established that photomediated polymerization led to reasonable cure rates for our thiocarbonylthio containing resins, we then applied our resin to a 3D printing setup. For all 3D printing conducted in this work, a DLP 3D printer was used to spatially confine the material formation via digital masking of the green LED light source ($\lambda_{max}$ = 525 nm, $I_0 = 0.32\ mW\,cm^{-2}$). A full description of the printing setup and procedures can be found in the Supporting information, Methods. Initially, three different resin formulations with varying ratios of [DMAm]:[PEGDA] and fixed concentrations of BTPA, EB, and TEtOHA were used to print a simple rectangular prism with dimensions 40 × 13 × 1.6 mm (l, w, t). These objects were printed using a layer slicing thickness of 20 μm and a layer cure time of 13 s. The storage modulus ($E'$) and glass transition temperature ($T_g$) of the printed materials were then determined by dynamic mechanical analysis (DMA) by performing a temperature ramp from −50 °C to 100 °C at a frequency of 1 Hz (Figure 2D). $E'$ was calculated at room temperature (≈20 °C), while $T_g$ was taken as the maximum of the Tan $\delta$ curve at a frequency of 1 Hz. As shown in Figure 2A, the samples printed in bulk with [DMAm]:[PEGDA] ratios of 30:70, 40:60, and 50:50, all showed similar $E'$ values in the range of 250 MPa at 20 °C. The $T_g$ for the 30:70, 40:60, and 50:50 [DMAm]:[PEGDA] systems was 30, 31, and 33, respectively. This increase in $T_g$ with the increase of DMAm concentration was expected given the relatively high $T_g$ of DMAm (≈90 °C) compared to typical PEG based acrylates ($T_g$ typically less than 0 °C).[22] The samples printed with a higher mole fraction of PEGDA (i.e., 30:70 DMAm:PEGDA) resulted in 3D materials with slightly sharper features. Therefore, the DMAm : PEGDA ratio was fixed at 30:70 for subsequent tests.

We then examined the effect of the BTPA concentration on the mechanical properties of the 3D printed materials. As the thiocarbonylthio species plays a vital role in mediating the radical polymerization process, we expected that altering its concentration would change the network structure, and in turn, the resultant material properties. As shown in Figure 2B, increasing the concentration of BTPA from 0, 8.96, 22.39, and 44.79 mmol per kg of resin (0, 100, 250, and 500 equivalents to EB) significantly reduced the $E'$ as well as the $T_g$. The reduced stiffness in the materials containing a higher concentration of BTPA was ascribed to the correspondingly lower segmental molecular weight between crosslinks and higher concentration of chain ends; as described by Flory, Fox, and Stockmayer, these networks have a higher free volume, and thus lower modulus and $T_g$.[23] Notably, a range of functional groups, including trithiocarbonates, have been utilized for the formation and rearrangement of crosslinked networks, as well as for producing shape-memory and self-healing materials, and even to induce permanent phase changes of polymeric materials.[24] The inclusion of these trithiocarbonate species thus allows controlled tuning of the material mechanical properties based on their concentrations. We subsequently investigated the build rate of our 3D printed materials. The model system used to fabricate the 3D printed objects in the previous section used a layer slicing thickness of 20 μm and a total layer cure time of 13 s, resulting in a build rate of $0.55\ cm\,h^{-1}$. Using the same resin formulation, the slicing thickness was then increased to 100 μm and the cure time per layer was changed to 13, 20, 25, and 30 s, which led to ill-defined objects, except for the system that used a 30 s exposure time (Supporting information, Figure S6). Under these conditions the build rate was increased to $1.2\ cm\,h^{-1}$.

 © 2019 Wiley-VCH Verlag GmbH & Co. KGaA, Weinheim 

15213773, 2019, 50, Downloaded from https://onlinelibrary.wiley.com/doi/10.1002/anie.201912608 by University Of New England, Wiley Online Library on [20/07/2023]. See the Terms and Conditions (https://onlinelibrary.wiley.com/terms-and-conditions) on Wiley Online Library for rules of use; OA articles are governed by the applicable Creative Commons License

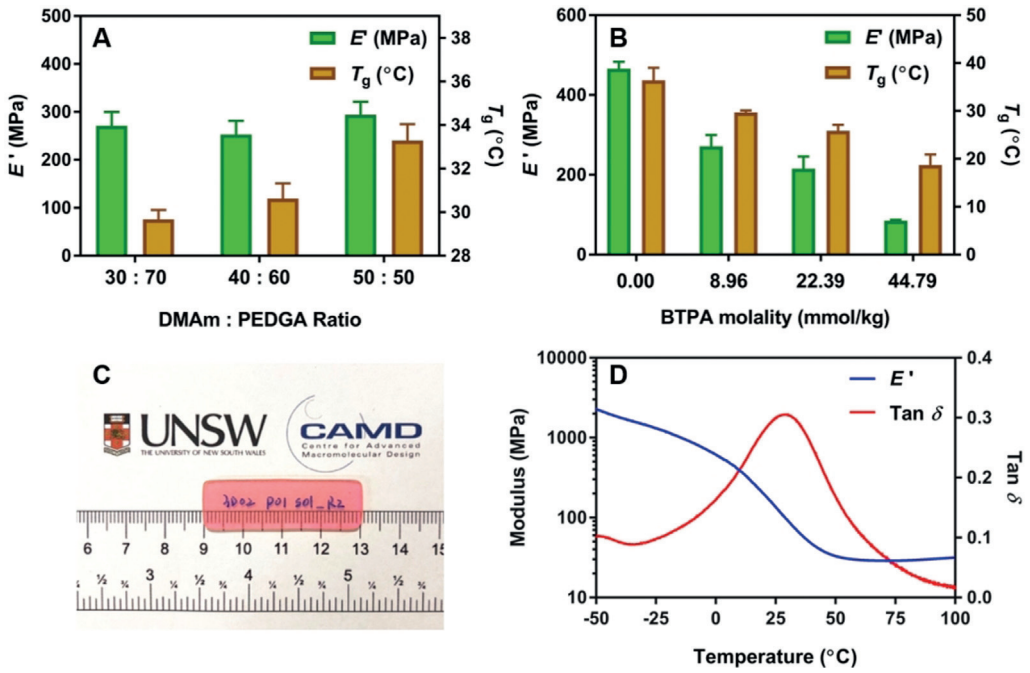


***Figure 2.*** Samples 3D printed with photocontrolled RAFT polymerization. A) Effect of changing the DMAm : PEGDA ratio on the storage modulus ($E'$) and glass transition temperature ($T_g$), while holding the EB, BTPA, and TEtOHA concentrations constant; B) effect of changing RAFT concentrations using a ratio [EB]:[DMAm]:[PEGDA]:[BTPA]:[TEtOHA] = 0.01:164:331:variable:20 in bulk; C) sample printed with a layer thickness of 20 μm and cure time per layer of 13 s using a recipe of [EB]:[DMAm]:[PEGDA]:[BTPA]:[TEtOHA] = 0.01:164:331:1:20; D) Storage modulus ($E'$) and Tan $\delta$ for sample shown in Figure 2C at a frequency of 1 Hz determined by DMA. Error bars were calculated using duplicate samples.

Similarly, a layer cure time of 20 s was required to form well-defined objects when the slicing thickness per layer was reduced to 50 μm. As expected, changing the total light dose by altering the slicing thickness and cure time per layer affected the resulting $E'$ and $T_g$ of the 3D printed materials. For instance, increasing the layer cure time while holding the layer slicing thickness constant led to stiffer materials (Supporting information, Figure S7). At a slicing thickness of 100 μm and layer cure time of 30 s the resulting $E'$ was 100 MPa, while at a slicing thickness of 100 μm and layer cure time of 40 s the $E'$ of the resulting material was 161 MPa. Additionally, printed materials that were post-cured through irradiation under green light ($\lambda_{max} = 525$ nm, $I_0 = 4.3$ mW cm$^{-2}$) showed increasing $E'$ and $T_g$ values up to 6 h post-cure time, which further demonstrated the ability for the mechanical properties of these materials to be manipulated via the irradiation parameters (Supporting information, Figure S8).

### *4D-printed materials through spatially controlled aqueous photopolymerization*

Spatially controlled light intensities have been previously explored by several groups for controlling the mechanical properties of 3D materials prepared by conventional photopolymerization, and even for 4D printing via swelling and dehydration induced actuation.[3e,25] As the mechanical properties of our 3D printed materials were dependent on the light exposure, we decided to exploit these differences to print a material with spatially resolved properties. Furthermore, our resin formulations were water soluble, which allowed objects to be printed in aqueous solutions. To date, only a handful of aqueous 3D printing systems have been developed[26] due to the insolubility of typical photoinitiators and monomers in water, however, the current system tailors toward 3D bioprinting due to the high biocompatibility of aqueous systems.[3h,m,n,27] To demonstrate the utility of our formulation, a hydrogel with spatially resolved properties was 3D printed and subsequently dehydrated and re-swelled for actuation; as such, a 4D printed material was fabricated using our photosensitive resin. A cross shaped object with spatially resolved properties based on the light dose to each layer was designed as shown in Figure 3A, and printed using a ratio of [EB]:[DMAm]:[PEGDA]:[BTPA]:[TEtOHA] = 0.01:1000:50:1:20 in a 50 wt-% solution of water. Using this geometry, the first layer was printed with a layer slicing thickness of 20 μm and a cure time 150 s, corresponding to a total dose of 108.0 mJ, while the subsequent 20 μm layers (99 layers) were exposed to green light for only 13 s, resulting in lower dose of light (9.4 mJ per layer). The cross was then placed in a water filled petri dish with the layer exposed to the higher light dose facing down; the cross started to deform as the layer with the higher cure time was swollen with water (Figure 3C and Supplementary Video 1). Subsequently, the cross was removed from the petri dish, flipped (Figure 3D), and exposed to a slow stream of compressed air to induce evaporation. Correspondingly, the arched cross flattened and then inverted its arch as the material dehydrated (Figure 3E,F).

 © 2019 Wiley-VCH Verlag GmbH & Co. KGaA, Weinheim 

15213773, 2019, 50, Downloaded from https://onlinelibrary.wiley.com/doi/10.1002/anie.201912608 by University Of New England, Wiley Online Library on [20/07/2023]. See the Terms and Conditions (https://onlinelibrary.wiley.com/terms-and-conditions) on Wiley Online Library for rules of use; OA articles are governed by the applicable Creative Commons License

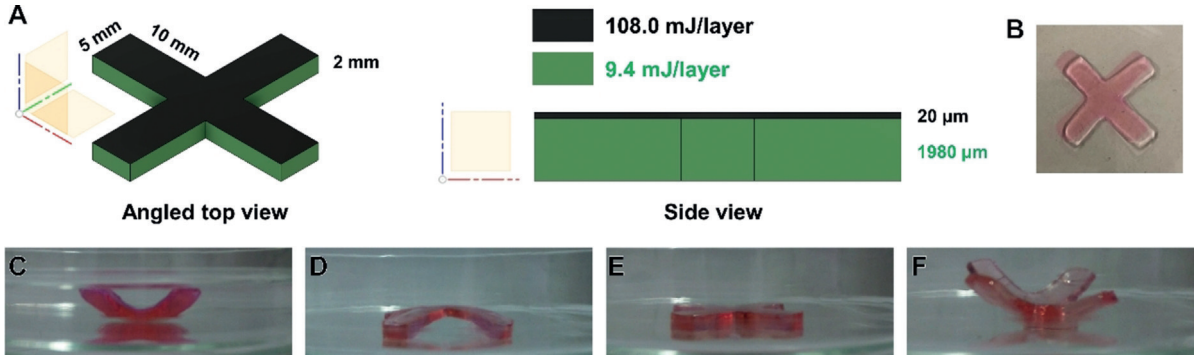


*Figure 3.* Swelling and desolvation induced actuation of a material 3D printed with spatially resolved light doses. A) Designed geometrical properties of cross; B) top view of swollen cross geometry (layer exposed to higher light dose on bottom of object); C) cross with layer exposed to higher light dose on the bottom, after 5 mins in water; D) flipped swollen cross before dehydration (layer exposed to higher light dose on top); E) cross after 80 seconds of dehydration; F) cross after 7 mins of dehydration (see Supplementary Video 1).

### *Reactivation of trithiocarbonate groups for the modification of 3D-printed materials*

Interestingly, our pink colored 3D printed materials changed color after post-curing under green light irradiation, resulting in materials that displayed a yellow hue (Figure 4A). To verify that the yellow color was the remaining RAFT agent in the 3D printed materials, UV-vis spectroscopy was used to analyze films printed using our resins in both the absence and presence of BTPA. Figure 4B shows the UV-vis spectra for films before and after a 45 min post-curing process under 4.3 mW cm$^{-2}$ green light irradiation. Both films printed in the presence and absence of BTPA displayed the typical EB absorption peak around 540 nm which disappeared after post-curing, however, only the film containing BTPA displayed and additional peak at 435 nm both before and after the photoinduced post-curing process.[20] This peak corresponds to the spin forbidden n → π* transition of the thiocarbonyl group, and demonstrates the retention of the BTPA end group in our materials.[8b]

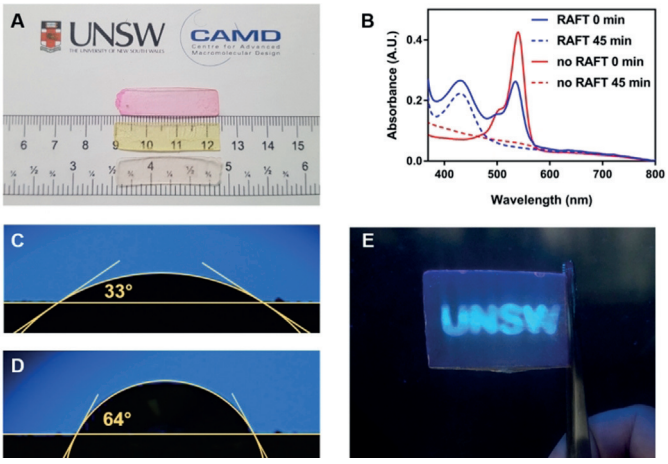


*Figure 4.* Secondary polymerization from 3D printed materials to change the surface properties. A) Color change in 3D printed films via post-curing under green light irradiation. From top: 3D printed film before post curing, after post-curing for BTPA containing resins, and after post-curing for RAFT agent-free resins; B) absorbance spectra before and after post-curing for films 3D printed in the presence and absence of RAFT agents; C) high surface wettability of 3D printed DMAm/PEDGA networks; D) decreased surface wettability for *n*BA functionalized material; E) spatially resolved fluorescence of 3D printed materials containing RAFT agent through photoinduced surface-functionalization in the presence of pyrene-MMA.

The ability to reinitiate polymerization from dormant thiocarbonylthio end-groups in the presence of diverse monomers has allowed multifunctional polymeric materials with diverse architectures to be synthesized in a straightforward manner. Moreover, surface initiated RAFT polymerization enables facile manipulation of surface properties. Indeed, many groups have investigated the initiation of surface tethered thiocarbonylthio species to impart functionality on the surface of materials.[28] As our 3D printed materials contained thiocarbonylthio species throughout the network as well as on the surface, we posited that we could post-functionalize our materials via a secondary photopolymerization process to change the surface properties. To demonstrate this concept, we 3D printed a rectangular prism with dimensions of 50 × 30 × 2 mm using a recipe of [EB]:[DMAm]:[PEGDA]:[BTPA]:[TEtOHA] = 0.01:164:331:5:20. The monomers used during the 3D printing process provided a hydrophilic surface with high wettability (contact angle = 33°), as shown in Figure 4C. Following fabrication, the 3D printed object was thoroughly washed with ethanol and the reaction mixture in the 3D printer vat was then switched to an *n*-butylacrylate (*n*BA) solution containing EB with a ratio of [EB]:[*n*BA] = 0.01:1000 and a small amount of ethanol (1.2 vol-%) to help solubilize the EB. The vat was then irradiated with 0.32 mW cm$^{-2}$ green light for 5 mins to induce polymerization on the surface of the hydrophilic network and change the surface properties. As shown in Figure 4D, the 3D printed material displayed a lower surface wettability following the secondary polymerization process, as demonstrated by a higher water contact angle (64°). As such, the surface properties of our 3D printed materials were altered after the secondary polymerization process, which is also in agreement with works very recently published by our groups.[14]

To further demonstrate the ability to change the surface properties of our RAFT containing 3D printed materials, a spatially controlled polymerization process using fluorescent monomers was performed.[14a] A DMAm/PEGDA net-


© 2019 Wiley-VCH Verlag GmbH & Co. KGaA, Weinheim


15213773, 2019, 50, Downloaded from https://onlinelibrary.wiley.com/doi/10.1002/anie.201912608 by University Of New England, Wiley Online Library on [20/07/2023]. See the Terms and Conditions (https://onlinelibrary.wiley.com/terms-and-conditions) on Wiley Online Library for rules of use; OA articles are governed by the applicable Creative Commons License

work was fabricated and subsequently exposed to green light irradiation in the presence of 1-pyrene methylmethacrylate (pyrene-MMA), DMAm, and EB ([EB]:[pyrene-MMA]:[DMAm] = 0.01:20:980). The spatially controlled irradiation was demonstrated in the form of letters spelling "UNSW" across the material surface. Following 10 min irradiation, the 3D printed material was removed from the build stage and carefully washed three times with a 1/1 volume mixture of DMSO/ethanol and irradiated with UV light ($\lambda = 312$ nm) to determine if the pyrene-MMA was successfully attached to the surface of the 3D printed material. As shown in Figure 4E, the 3D printed material showed strong fluorescence only in the "UNSW" region that was exposed to light during the secondary photopolymerization, thus indicating a spatially controlled functionalization from the RAFT agent on the surface of our 3D printed materials, which has also recently been used for a similar system published in the literature by our groups (Supporting Information, Figure S9).[14a]

## Conclusion

In summary, we have developed a water soluble and environmentally friendly photocurable resin containing thiocarbonylthio compounds for application to 3D and 4D printing processes. The use of the organic dye EB in conjunction with triethanolamine as co-catalyst and BTPA as RAFT agent allowed build speeds up to 1.2 cm $h^{-1}$, and provided a platform for photoinduced 3D printing in aqueous solutions under benign, low energy green light irradiation; these systems thus tailor toward 3D-bioprinting applications. Remarkably, the ability to spatially control the dose of light applied during the 3D printing process provided stimuli-responsive materials in a one-pass fabrication process, as demonstrated by swelling and dehydration induced actuation of a 4D printed hydrogel. The spatially controlled properties conferred on these hydrogels demonstrate the first 4D printing using a RDRP process. More importantly, the retention of the RAFT functionality during the 3D printing process allowed the 3D printed materials to be easily post-modified after printing. The reinitiation of dormant RAFT agents on the surface of the 3D printed hydrophilic network structure was demonstrated by chain extension with a hydrophobic monomer, which resulted in an increase in surface hydrophobicity. Surface functionalization of the 3D printed material was also able to be spatially confined through selected irradiation during the post-functionalization. The versatility of this photomediated RAFT polymerization process provides access to a range of new functional and stimuli-responsive materials which can be applied for the design of biocompatible materials.

## Conflict of interest

The authors declare no conflict of interest.

**Keywords:** 3D printing · 4D printing · functional materials · photopolymerization · RAFT polymerization

**How to cite:** *Angew. Chem. Int. Ed.* **2019**, *58*, 17954 – 17963
*Angew. Chem.* **2019**, *131*, 18122 – 18131

[1] a) M. R. Hartings, Z. Ahmed, *Nat. Rev. Chem.* **2019**, *3*, 305 – 314; b) S. H. Huang, P. Liu, A. Mokasdar, L. Hou, *Int. J. Adv. Manuf. Technol.* **2013**, *67*, 1191 – 1203; c) B. C. Gross, J. L. Erkal, S. Y. Lockwood, C. Chen, D. M. Spence, *Anal. Chem.* **2014**, *86*, 3240 – 3253; d) J. W. Stansbury, M. J. Idacavage, *Dent. Mater.* **2016**, *32*, 54 – 64; e) S. C. Ligon, R. Liska, J. Stampfl, M. Gurr, R. Mülhaupt, *Chem. Rev.* **2017**, *117*, 10212 – 10290.

[2] a) C. Barner-Kowollik, M. Bastmeyer, E. Blasco, G. Delaittre, P. Müller, B. Richter, M. Wegener, *Angew. Chem. Int. Ed.* **2017**, *56*, 15828 – 15845; *Angew. Chem.* **2017**, *129*, 16038 – 16056; b) J. Zhang, P. Xiao, *Polym. Chem.* **2018**, *9*, 1530 – 1540; c) A. J. Boydston, B. Cao, A. Nelson, R. J. Ono, A. Saha, J. J. Schwartz, C. J. Thrasher, *J. Mater. Chem. A* **2018**, *6*, 20621 – 20645; d) X. Kuang, D. J. Roach, J. Wu, C. M. Hamel, Z. Ding, T. Wang, M. L. Dunn, H. J. Qi, *Adv. Funct. Mater.* **2019**, *29*, 1805290; e) C. W. Hull, U.S. Patent, 4575330A, **1986**; f) Q. Mu, L. Wang, C. K. Dunn, X. Kuang, F. Duan, Z. Zhang, H. J. Qi, T. Wang, *Addit. Manuf.* **2017**, *18*, 74 – 83; g) A. Bagheri, J. Jin, *ACS Appl. Polym. Mater.* **2019**, *1*, 593 – 611; h) S. Chatani, C. J. Kloxin, C. N. Bowman, *Polym. Chem.* **2014**, *5*, 2187 – 2201; i) N. Corrigan, J. Yeow, P. Judzewitsch, J. Xu, C. Boyer, *Angew. Chem. Int. Ed.* **2019**, *58*, 5170 – 5189; *Angew. Chem.* **2019**, *131*, 5224 – 5243.

[3] a) M. M. Zieger, P. Müller, E. Blasco, C. Petit, V. Hahn, L. Michalek, H. Mutlu, M. Wegener, C. Barner-Kowollik, *Adv. Funct. Mater.* **2018**, *28*, 1801405; b) D. Gräfe, A. Wickberg, M. M. Zieger, M. Wegener, E. Blasco, C. Barner-Kowollik, *Nat. Commun.* **2018**, *9*, 2788; c) N. D. Dolinski, Z. A. Page, E. B. Callaway, F. Eisenreich, R. V. Garcia, R. Chavez, D. P. Bothman, S. Hecht, F. W. Zok, C. J. Hawker, *Adv. Mater.* **2018**, *30*, 1800364; d) J. J. Schwartz, A. J. Boydston, *Nat. Commun.* **2019**, *10*, 791; e) G. I. Peterson, J. J. Schwartz, D. Zhang, B. M. Weiss, M. A. Ganter, D. W. Storti, A. J. Boydston, *ACS Appl. Mater. Interfaces* **2016**, *8*, 29037 – 29043; f) B. Zhang, K. Kowsari, A. Serjouei, M. L. Dunn, Q. Ge, *Nat. Commun.* **2018**, *9*, 1831; g) B. J. Adzima, C. J. Kloxin, C. A. DeForest, K. S. Anseth, C. N. Bowman, *Macromol. Rapid Commun.* **2012**, *33*, 2092 – 2096; h) S. H. Kim, Y. K. Yeon, J. M. Lee, J. R. Chao, Y. J. Lee, Y. B. Seo, M. T. Sultan, O. J. Lee, J. S. Lee, S.-i. Yoon, I.-S. Hong, G. Khang, S. J. Lee, J. J. Yoo, C. H. Park, *Nat. Commun.* **2018**, *9*, 1620; i) B. E. Kelly, I. Bhattacharya, H. Heidari, M. Shusteff, C. M. Spadaccini, H. K. Taylor, *Science* **2019**, 363, 1075; j) M. Shusteff, A. E. M. Browar, B. E. Kelly, J. Henriksson, T. H. Weisgraber, R. M. Panas, N. X. Fang, C. M. Spadaccini, *Sci. Adv.* **2017**, *3*, eaao5496; k) J. R. Tumbleston, D. Shirvanyants, N. Ermoshkin, R. Janusziewicz, A. R. Johnson, D. Kelly, K. Chen, R. Pinschmidt, J. P. Rolland, A. Ermoshkin, E. T. Samulski, J. M. DeSimone, *Science* **2015**, *347*, 1349; l) Z. C. Eckel, C. Zhou, J. H. Martin, A. J. Jacobsen, W. B. Carter, T. A. Schaedler, *Science* **2016**, *351*, 58; m) H. Yin, Y. Ding, Y. Zhai, W. Tan, X. Yin, *Nat. Commun.* **2018**, *9*, 4096; n) R. J. Mondschein, A. Kanitkar, C. B. Williams, S. S. Verbridge, T. E. Long, *Biomaterials* **2017**, *140*, 170 – 188; o) F. Kotz, K. Arnold, W. Bauer, D. Schild, N. Keller, K. Sachsenheimer, T. M. Nargang, C. Richter, D. Helmer, B. E. Rapp, *Nature* **2017**, *544*, 337.

[4] Q. Ge, A. H. Sakhaei, H. Lee, C. K. Dunn, N. X. Fang, M. L. Dunn, *Sci. Rep.* **2016**, *6*, 31110.

[5] a) C. Boyer, N. A. Corrigan, K. Jung, D. Nguyen, T.-K. Nguyen, N. N. M. Adnan, S. Oliver, S. Shanmugam, J. Yeow, *Chem. Rev.* **2016**, *116*, 1803 – 1949; b) G. Moad, E. Rizzardo, S. H. Thang, *Aust. J. Chem.* **2012**, *65*, 985 – 1076; c) C. J. Hawker, *J. Am.*

 © 2019 Wiley-VCH Verlag GmbH & Co. KGaA, Weinheim 

15213773, 2019, 50, Downloaded from https://onlinelibrary.wiley.com/doi/10.1002/anie.201912608 by University Of New England, Wiley Online Library on [20/07/2023]. See the Terms and Conditions (https://onlinelibrary.wiley.com/terms-and-conditions) on Wiley Online Library for rules of use; OA articles are governed by the applicable Creative Commons License

*Chem. Soc.* **1994**, *116*, 11185 – 11186; d) J.-S. Wang, K. Matyjaszewski, *J. Am. Chem. Soc.* **1995**, *117*, 5614 – 5615; e) W. A. Braunecker, K. Matyjaszewski, *Prog. Polym. Sci.* **2007**, *32*, 93 – 146; f) S. Perrier, P. Takolpuckdee, *J. Polym. Sci. Part A* **2005**, *43*, 5347 – 5393; g) S. Shanmugam, K. Matyjaszewski in *Reversible Deactivation Radical Polymerization: Mechanisms and Synthetic Methodologies*, *Vol. 1284*, American Chemical Society, Washington, **2018**, pp. 1 – 39.

[6] a) C. Barner-Kowollik, *Handbook of RAFT polymerization*, Wiley, Hoboken, **2008**; b) J. Chiefari, Y. Chong, F. Ercole, J. Krstina, J. Jeffery, T. P. Le, R. T. Mayadunne, G. F. Meijs, C. L. Moad, G. Moad, *Macromolecules* **1998**, *31*, 5559 – 5562; c) S. Perrier, *Macromolecules* **2017**, *50*, 7433 – 7447; d) C. J. Hawker, A. W. Bosman, E. Harth, *Chem. Rev.* **2001**, *101*, 3661 – 3688.

[7] M. R. Hill, R. N. Carmean, B. S. Sumerlin, *Macromolecules* **2015**, *48*, 5459 – 5469.

[8] a) J. Xu, S. Shanmugam, N. A. Corrigan, C. Boyer in *Controlled Radical Polymerization: Mechanisms*, *Vol. 1187*, American Chemical Society, Washington, **2015**, pp. 247 – 267; b) T. G. McKenzie, Q. Fu, E. H. H. Wong, D. E. Dunstan, G. G. Qiao, *Macromolecules* **2015**, *48*, 3864 – 3872.

[9] a) S. Shanmugam, J. Xu, C. Boyer, *J. Am. Chem. Soc.* **2015**, *137*, 9174 – 9185; b) N. Corrigan, D. Rosli, J. W. J. Jones, J. Xu, C. Boyer, *Macromolecules* **2016**, *49*, 6779 – 6789; c) J. Xu, K. Jung, A. Atme, S. Shanmugam, C. Boyer, *J. Am. Chem. Soc.* **2014**, *136*, 5508 – 5519; d) S. Shanmugam, J. Xu, C. Boyer, *Chem. Sci.* **2015**, *6*, 1341 – 1349; e) S. Shanmugam, J. Xu, C. Boyer, *Angew. Chem. Int. Ed.* **2016**, *55*, 1036 – 1040; *Angew. Chem.* **2016**, *128*, 1048 – 1052; f) L. Zhang, C. Wu, K. Jung, Y. H. Ng, C. Boyer, *Angew. Chem. Int. Ed.* **2019**, https://doi.org/10.1002/anie.201909014; *Angew. Chem.* **2019**, https://doi.org/10.1002/ange.201909014.

[10] a) N. Corrigan, J. Xu, C. Boyer, X. Allonas, *ChemPhotoChem* **2019**, https://doi.org/10.1002/cptc.201800182; b) P. Seal, J. Xu, S. De Luca, C. Boyer, S. C. Smith, *Adv. Theory Simul.* **2019**, *2*, 1900038.

[11] a) M. Chen, Y. Gu, A. Singh, M. Zhong, A. M. Jordan, S. Biswas, L. T. J. Korley, A. C. Balazs, J. A. Johnson, *ACS Cent. Sci.* **2017**, *3*, 124 – 134; b) H. Zhou, J. A. Johnson, *Angew. Chem. Int. Ed.* **2013**, *52*, 2235 – 2238; *Angew. Chem.* **2013**, *125*, 2291 – 2294; c) J. Cuthbert, A. Beziau, E. Gottlieb, L. Fu, R. Yuan, A. C. Balazs, T. Kowalewski, K. Matyjaszewski, *Macromolecules* **2018**, *51*, 3808 – 3817; d) S. Shanmugam, J. Cuthbert, J. Flum, M. Fantin, C. Boyer, T. Kowalewski, K. Matyjaszewski, *Polym. Chem.* **2019**, *10*, 2477 – 2483; e) A. Bagheri, C. Bainbridge, J. Jin, *ACS Appl. Polym. Mater.* **2019**, *1*, 1896 – 1904; f) M. W. Lampley, E. Tsogtgerel, E. Harth, *Polym. Chem.* **2019**, *10*, 3841 – 3850; g) S. Shanmugam, J. Xu, C. Boyer, *ACS Cent. Sci.* **2017**, *3*, 95 – 96.

[12] Y. Amamoto, J. Kamada, H. Otsuka, A. Takahara, K. Matyjaszewski, *Angew. Chem. Int. Ed.* **2011**, *50*, 1660 – 1663; *Angew. Chem.* **2011**, *123*, 1698 – 1701.

[13] M. B. Gordon, J. M. French, N. J. Wagner, C. J. Kloxin, *Adv. Mater.* **2015**, *27*, 8007 – 8010.

[14] a) A. Bagheri, K. E. Engel, C. Bainbridge, J. Xu, C. Boyer, J. Jin, *Polym. Chem.* **2019**, https://doi.org/10.1039/C9PY01419E; b) A. Bagheri, C. Bainbridge, K. E. Engel, G. Qiao, J. Xu, C. Boyer, J. Jin, *ChemRxiv*, https://doi.org/10.26434/chemrxiv.10116122 (published online 07/11/2019).

[15] a) J. Xu, S. Shanmugam, H. T. Duong, C. Boyer, *Polym. Chem.* **2015**, *6*, 5615 – 5624; b) C. Wu, N. Corrigan, C.-H. Lim, K. Jung, J. Zhu, G. Miyake, J. Xu, C. Boyer, *Macromolecules* **2019**, *52*, 236 – 248; c) N. Corrigan, L. Zhernakov, M. H. Hashim, J. Xu, C. Boyer, *React. Chem. Eng.* **2019**, *4*, 1216 – 1228; d) C. A. Figg, J. D. Hickman, G. M. Scheutz, S. Shanmugam, R. N. Carmean, B. S. Tucker, C. Boyer, B. S. Sumerlin, *Macromolecules* **2018**, *51*, 1370 – 1376; e) N. Zaquen, A. M. N. B. P. H. A. Kadir, A. Iasa, N. Corrigan, T. Junkers, P. B. Zetterlund, C. Boyer, *Macromolecules* **2019**, *52*, 1609 – 1619; f) S. Shanmugam, S. Xu, N. N. M. Adnan, C. Boyer, *Macromolecules* **2018**, *51*, 779 – 790.

[16] a) H. J. Avens, E. L. Chang, A. M. May, B. J. Berron, G. J. Seedorf, V. Balasubramaniam, C. N. Bowman, *J. Nanopart. Res.* **2011**, *13*, 331 – 346; b) H. J. Avens, C. N. Bowman, *Acta Biomater.* **2010**, *6*, 83 – 89; c) H. J. Avens, C. N. Bowman, *J. Polym. Sci. Part A* **2009**, *47*, 6083 – 6094; d) H. J. Avens, T. J. Randle, C. N. Bowman, *Polymer* **2008**, *49*, 4762 – 4768; e) J. Hu, J. Wang, T. H. Nguyen, N. Zheng, *Beilstein J. Org. Chem.* **2013**, *9*, 1977 – 2001; f) S. Kızılel, V. H. Pérez-Luna, F. Teymour, *Langmuir* **2004**, *20*, 8652 – 8658; g) D. P. Hari, B. König, *Chem. Commun.* **2014**, *50*, 6688 – 6699.

[17] B. Nomeir, O. Fabre, K. Ferji, *Macromolecules* **2019**, *52*, 6898 – 6903.

[18] Q. Fu, K. Xie, T. G. McKenzie, G. G. Qiao, *Polym. Chem.* **2017**, *8*, 1519 – 1526.

[19] a) J. Yeow, R. Chapman, A. J. Gormley, C. Boyer, *Chem. Soc. Rev.* **2018**, *47*, 4357 – 4387; b) S. C. Ligon, B. Husár, H. Wutzel, R. Holman, R. Liska, *Chem. Rev.* **2014**, *114*, 557 – 589; c) C. N. Bowman, C. J. Kloxin, *AIChE J.* **2008**, *54*, 2775 – 2795; d) K. K. Childress, K. Kim, D. J. Glugla, C. B. Musgrave, C. N. Bowman, J. W. Stansbury, *Macromolecules* **2019**, *52*, 4968 – 4978.

[20] A. Aguirre-Soto, K. Kaastrup, S. Kim, K. Ugo-Beke, H. D. Sikes, *ACS Catal.* **2018**, *8*, 6394 – 6400.

[21] S. C. Ligon-Auer, M. Schwentenwein, C. Gorsche, J. Stampfl, R. Liska, *Polym. Chem.* **2016**, *7*, 257 – 286.

[22] a) J. Brandrup, E. H. Immergut, E. A. Grulke, A. Abe, D. R. Bloch, *Polymer handbook*, *Vol. 89*, Wiley, New York, **1999**; b) S. Krause, J. J. Gormley, N. Roman, J. A. Shetter, W. H. Watanabe, *J. Polym. Sci. Part A* **1965**, *3*, 3573 – 3586; c) H. Ju, B. D. McCloskey, A. C. Sagle, V. A. Kusuma, B. D. Freeman, *J. Membr. Sci.* **2009**, *330*, 180 – 188.

[23] a) P. J. Flory, *Principles of Polymer Chemistry*, Cornell University Press, Ithaca, **1953**; b) T. G. Fox, P. J. Flory, *J. Appl. Phys.* **1950**, *21*, 581 – 591; c) W. H. Stockmayer, *J. Chem. Phys.* **1943**, *11*, 45 – 55.

[24] a) C. J. Kloxin, C. N. Bowman, *Chem. Soc. Rev.* **2013**, *42*, 7161 – 7173; b) P. Chakma, D. Konkolewicz, *Angew. Chem. Int. Ed.* **2019**, *58*, 9682 – 9695; *Angew. Chem.* **2019**, *131*, 9784 – 9797; c) Y. Meng, C. R. Fenoli, A. Aguirre-Soto, C. N. Bowman, M. Anthamatten, *Adv. Mater.* **2014**, *26*, 6497 – 6502; d) C. M. Yakacki, R. Shandas, D. Safranski, A. M. Ortega, K. Sassaman, K. Gall, *Adv. Funct. Mater.* **2008**, *18*, 2428 – 2435; e) H. Y. Park, C. J. Kloxin, T. F. Scott, C. N. Bowman, *Macromolecules* **2010**, *43*, 10188 – 10190; f) A. Lendlein, H. Jiang, O. Jünger, R. Langer, *Nature* **2005**, *434*, 879; g) C. J. Kloxin, T. F. Scott, H. Y. Park, C. N. Bowman, *Adv. Mater.* **2011**, *23*, 1977 – 1981; h) C. J. Kloxin, T. F. Scott, C. N. Bowman, *Macromolecules* **2009**, *42*, 2551 – 2556; i) T. F. Scott, A. D. Schneider, W. D. Cook, C. N. Bowman, *Science* **2005**, *308*, 1615; j) S. Telitel, Y. Amamoto, J. Poly, F. Morlet-Savary, O. Soppera, J. Lalevée, K. Matyjaszewski, *Polym. Chem.* **2014**, *5*, 921 – 930; k) Y. Amamoto, H. Otsuka, A. Takahara, K. Matyjaszewski, *Adv. Mater.* **2012**, *24*, 3975 – 3980; l) Y. Amamoto, H. Otsuka, A. Takahara, K. Matyjaszewski, *ACS Macro Lett.* **2012**, *1*, 478 – 481; m) M. K. McBride, M. Hendrikx, D. Liu, B. T. Worrell, D. J. Broer, C. N. Bowman, *Adv. Mater.* **2017**, *29*, 1606509; n) B. T. Worrell, M. K. McBride, G. B. Lyon, L. M. Cox, C. Wang, S. Mavila, C.-H. Lim, H. M. Coley, C. B. Musgrave, Y. Ding, C. N. Bowman, *Nat. Commun.* **2018**, *9*, 2804; o) M. Gernhardt, E. Blasco, M. Hippler, J. Blinco, M. Bastmeyer, M. Wegener, H. Frisch, C. Barner-Kowollik, *Adv. Mater.* **2019**, *31*, 1901269.

[25] a) X. Kuang, J. Wu, K. Chen, Z. Zhao, Z. Ding, F. Hu, D. Fang, H. J. Qi, *Sci. Adv.* **2019**, *5*, eaav5790; b) K. L. Wiley, E. M. Ovadia, C. J. Calo, R. E. Huber, A. M. Kloxin, *Polym. Chem.* **2019**, *10*, 4428 – 4440; c) L. Huang, R. Jiang, J. Wu, J. Song, H. Bai, B. Li, Q. Zhao, T. Xie, *Adv. Mater.* **2017**, *29*, 1605390; d) Z.

 © 2019 Wiley-VCH Verlag GmbH & Co. KGaA, Weinheim 

15213773, 2019, 50, Downloaded from https://onlinelibrary.wiley.com/doi/10.1002/anie.201912608 by University Of New England, Wiley Online Library on [20/07/2023]. See the Terms and Conditions (https://onlinelibrary.wiley.com/terms-and-conditions) on Wiley Online Library for rules of use; OA articles are governed by the applicable Creative Commons License

Zhao, J. Wu, X. Mu, H. Chen, H. J. Qi, D. Fang, *Macromol. Rapid Commun.* **2017**, *38*, 1600625.
[26] a) A. A. Pawar, G. Saada, I. Cooperstein, L. Larush, J. A. Jackman, S. R. Tabaei, N.-J. Cho, S. Magdassi, *Sci. Adv.* **2016**, *2*, e1501381; b) A. A. Pawar, S. Halivni, N. Waiskopf, Y. Ben-Shahar, M. Soreni-Harari, S. Bergbreiter, U. Banin, S. Magdassi, *Nano Lett.* **2017**, *17*, 4497 – 4501.
[27] J. Niu, D. J. Lunn, A. Pusuluri, J. I. Yoo, M. A. O'Malley, S. Mitragotri, H. T. Soh, C. J. Hawker, *Nat. Chem.* **2017**, *9*, 537.
[28] a) M. D. Rowe-Konopacki, S. G. Boyes, *Macromolecules* **2007**, *40*, 879 – 888; b) R. Barbey, L. Lavanant, D. Paripovic, N. Schüwer, C. Sugnaux, S. Tugulu, H.-A. Klok, *Chem. Rev.* **2009**, *109*, 5437 – 5527; c) N. Luo, J. B. Hutchison, K. S. Anseth, C. N. Bowman, *J. Polym. Sci. Part A* **2002**, *40*, 1885 – 1891; d) M. Li, M. Fromel, D. Ranaweera, S. Rocha, C. Boyer, C. W. Pester, *ACS Macro Lett.* **2019**, *8*, 374 – 380.

Manuscript received: October 2, 2019
Accepted manuscript online: October 23, 2019
Version of record online: November 15, 2019

 © 2019 Wiley-VCH Verlag GmbH & Co. KGaA, Weinheim 

15213773, 2019, 50, Downloaded from https://onlinelibrary.wiley.com/doi/10.1002/anie.201912608 by University Of New England, Wiley Online Library on [20/07/2023]. See the Terms and Conditions (https://onlinelibrary.wiley.com/terms-and-conditions) on Wiley Online Library for rules of use; OA articles are governed by the applicable Creative Commons License